Mechanical and Thermal Properties of Metallic and Semiconductive Nanostructures

ARTICLE *in* THE JOURNAL OF PHYSICAL CHEMISTRY C · MARCH 2008

Impact Factor: 4.77 · DOI: 10.1021/Jp077371n

Mechanical and Thermal Properties of Metallic and Semiconductive Nanostructures

G. Guisbiers,*,† M. Kazan,† O. Van Overschelde,‡ M. Wautelet,‡ and S. Pereira†

CICECO, University of Aveiro, 3810-193 Aveiro, Portugal, and Physics of Condensed Matter, University of Mons-Hainaut, Avenue Maistriau 23, 7000 Mons, Belgium

Received: September 13, 2007; In Final Form: November 28, 2007

Using a top-down approach, we report a theoretical investigation of the melting temperature at the nanoscale, T_m, for different shapes of "free-standing" nanostructures. To easily calculate the nanoscale melting temperature for a wide range of metals and semiconductors, a convenient shape parameter called α_{shape} is defined. Considering this parameter, we argue why smaller size effects are observed in high bulk melting temperature materials. Using T_m, a phase transition stress model is proposed to evaluate the intrinsic strain and stress during the first steps of solidification. Then, the size effect on the Thornton & Hoffman's criterion at the nanoscale is discussed and the intrinsic residual stress determination in nanostructures is found to be essential for sizes below 100 nm. Furthermore, the inverse Hall-Petch effect, for sizes below ∼15 nm, can be understood by this model. Finally, the residual strain in hexagonal zinc oxide nanowires is calculated as a function of the wire dimensions.

1. Introduction

Materials with dimensions between 1 and 100 nm, i.e., nanomaterials, are under intense investigation worldwide due to their wide scientific and technological interest.[1,2] Irrespectively of their nature or functionality, these nanostructures are intrinsically characterized by a large ratio of surface atoms to volume atoms. This fact modifies some of the basic material physical properties which are well defined for bulk. A notable example of these size induced changes is that the melting temperatures of nanostructured materials are lower than those measured at the bulk.[3−7] The shape of the nanomaterial also influences the melting temperature since the ratio of the number of atoms at the surface relatively to those in the volume varies with the shape.

To study the melting temperature at the nanoscale, there are two approaches: bottom-up and top-down. The first makes use of computational methods like molecular dynamics,[8,9] whereas the second relies on classical thermodynamics.[10−24] Molecular dynamics, generally considers less than 100 000 atoms, in order to keep calculation times within reasonable values. This factor limits the nanostructure size modeled to a maximum size of tens of nm, but on the other hand, effects such as chemical environment on the melting temperature can be considered. Therefore, the top-down approach emerges as a simple complementary method that may provide useful insights in nanotechnology.

As a preamble for the subsequent discussion, one should note that thermodynamics, as a phenomenological theory, is strictly valid for macroscopic systems. To get a statistical limit of validity in terms of size for classical thermodynamics, we consider that the relative temperature fluctuation inside a cube $\delta T/T \approx (NL^3)^{(-1/2)}$ (where L^3 is the volume of the cube with N atoms per unit volume) is less than 3%. As shown previously in more detail,[19−21] this last strategy only allows nanostructures with sizes larger than ∼2 nm to be described. Hence, this is the lower size limit that we will consider within our framework.

The goal of the present work is to give a theoretical evaluation of size effects for a large number of metals and semiconductors, based on such top-down approach. In section 2, the melting temperature for different shapes of nanostructures is discussed, and the α_{shape} parameter is defined. This parameter allows to understand why smaller size effects are observed in high bulk melting temperature materials. In section 3, the validity of the Thornton & Hoffman's criterion at the nanoscale is discussed. In section 4, the phase transition stress model is presented to determine the intrinsic strain and stress during the first steps of solidification. In section 5, the results are discussed and compared to experimental data. Section 6 deals with conclusions and perspectives.

2. Melting Temperature of "Free-Standing" Nanostructures

2.1. Theory. Since the pioneering work of Pawlow in 1909,[10] the decrease of the melting temperature with the size is known. The melting−freezing transition at the nanoscale has been studied by molecular dynamics[8,9] as well as by thermodynamics.[10−24] In this paper, we study the size effects on the T_m for the following shapes: spherical nanoparticle, tetrahedral nanoparticle, cubic nanoparticle, cylindrical nanowire, parallelepiped nanowire, and hexagonal nanowire. Using classical thermodynamics, and applying the energy conservation law for a nanostructure at the melting phase transition, we get the melting temperature of a nanostructure:[19−21,23,24]

$$T_m = T_{m,\infty}\left[1 + \frac{(\gamma_l - \gamma_s)}{\Delta H_{m,\infty}}\frac{A}{V}\right] \quad (1)$$

$T_{m,\infty}$ is the bulk melting temperature of the considered bulk material [K], whereas γ_l and γ_s are the surface tensions* in the liquid and solid-phase, respectively [J/m^2], and finally $\Delta H_{m,\infty}$ represents the bulk melting enthalpy [J/m^3]. [At this point it is worthwhile to note the following: since a liquid surface is

* Corresponding author. E-mail: gregory.guisbiers@physics.org.
† University of Aveiro.
‡ University of Mons-Hainaut.

10.1021/jp077371n CCC: $40.75
Published on Web 02/22/2008

TABLE 1: Values of the α_{shape} Parameter for Different Shapes of Metallic Nanoparticles and Nanowires

			nanoparticle			nanowire ($h = 100$ nm)		
material	atomic no.	$T_{m,\infty}$ (K)	α_{sphere} (nm)	$\alpha_{tetrahedron}$ (nm)	α_{cubic} (nm)	$\alpha_{cylinder}$ (nm)	$\alpha_{parallelepiped}$ (nm)	$\alpha_{hexagonal}$ (nm)
Al	13	933	1.56	7.97	3.25	1.10	2.19	1.27
Sc	21	1814	2.40	11.76	4.80	1.62	3.23	1.88
Ti	22	1941	1.78	8.73	3.56	1.20	2.40	1.40
V	23	2183	1.56	7.64	3.12	1.05	2.10	1.22
Cr	24	2180	1.50	7.36	3.00	1.01	2.02	1.18
Mn	25	1519	1.61	7.89	3.22	1.09	2.17	1.26
Fe	26	1811	2.46	12.04	4.92	1.66	3.31	1.93
Co	27	1768	2.49	12.21	4.98	1.68	3.36	1.95
Ni	28	1728	1.56	7.65	3.13	1.06	2.10	1.22
Cu	29	1358	1.63	7.98	3.26	1.10	2.19	1.28
Zn	30	693	1.32	6.45	2.63	0.89	1.77	1.03
Y	39	1795	2.34	11.47	4.68	1.58	3.15	1.83
Zr	40	2128	1.91	9.34	3.81	1.29	2.57	1.49
Nb	41	2750	1.51	7.39	3.02	1.02	2.03	1.18
Mo	42	2893	1.06	5.19	2.12	0.71	1.43	0.83
Ru	44	2607	1.03	5.03	2.05	0.69	1.38	0.80
Rh	45	2237	1.33	6.51	2.66	0.90	1.79	1.04
Pd	46	1828	1.68	8.25	3.37	1.14	2.27	1.32
Ag	47	1235	1.88	9.22	3.76	1.27	2.54	1.47
Cd	48	594	2.36	11.54	4.71	1.59	3.17	1.85
In	49	430	3.79	18.57	7.58	2.56	5.11	2.97
$Sn_{(\beta)}$	50	505	2.04	10.01	4.09	1.38	2.75	1.60
Hf	72	2506	1.63	7.97	3.26	1.10	2.19	1.28
Ta	73	3290	1.56	7.64	3.12	1.05	2.10	1.22
W	74	3693	1.26	6.21	2.53	0.86	1.71	0.99
Re	75	3458	1.50	7.37	3.01	1.02	2.02	1.18
Os	76	3306	0.83	4.08	1.66	0.56	1.12	0.65
Ir	77	2719	0.97	4.73	1.93	0.65	1.30	1.76
Pt	78	2042	1.52	7.44	3.04	1.03	2.05	1.19
Au	79	1337	1.83	8.96	3.66	1.24	2.46	1.43
Hg	80	234	4.41	21.57	8.80	2.97	5.93	3.45
Tl	81	577	3.55	17.38	7.09	2.40	4.78	2.78
Pb	82	601	2.90	14.21	5.80	1.96	3.91	2.27

characterized by the single quantity γ, which is both the energy for creation of a unit surface area (i.e., the surface energy) and the quantity responsible to capillarity effects of the Laplace pressure type, the term "surface tension" is widely used for the surface energy γ. Mainly for historical reasons, the use of this term has been extended to the surfaces and interfaces of solids. We will not make a distinction between the "surface energy" and the "intrinsic surface stress" and use the term "surface tension" for solids also.] The ratio A/V, the surface area divided by the volume, determines the relation between the number of atoms on the surface over the number of atoms inside the volume of the nanostructure. To calculate the size effect on the melting temperature, we use the bulk values of the surface tension, melting enthalpy and do not consider the size dependencies of these properties : γ_l, γ_s, and $\Delta H_{m,\infty}$. This is justified by the fact that the size effect on the surface tension[25] and melting enthalpy[26,27] are less than ~4% and ~10%, respectively, for sizes higher than 10 nm.

To characterize the size effect on the melting temperature only with one parameter, let us rewrite eq 1 as

$$T_m = T_{m,\infty}\left(1 - \frac{\alpha_{shape}}{2L}\right) \quad (2)$$

where $\alpha_{shape} = 2AL(\gamma_s - \gamma_l)/(V\Delta H_{m,\infty})$. The parameter L represents the length size of the nanostructure, i.e., the radius for the case of a spherical structure, or the length side for nonspherical structures. For a given material, α_{shape} quantifies the size effect on the bulk melting temperature, and since this parameter depends only on the shape, it is called the shape parameter. The α_{shape} expression can be simplified if the ratio A/V is expressed as function of L^{-1}. The shape parameter is always positive, except when a surfusion phenomenon occurs, and it depends of the liquid/solid surface tension and the bulk melting enthalpy.

2.2. Discussion Concerning the Preferentially Adopted Shape. Previous work[18−21,28] deals with nanostructures supported by silicon substrates, the work here gives the α_{shape} for "free-standing" nanostructures. For all of the materials given in the Tables 1 and 2 (metals, semiconductors, and binary semiconductors), we calculated this parameter for the following shapes: sphere, tetrahedron, cube, cylinder, parallelepiped, and hexagon. The values of liquid and solid surface tensions and the melting enthalpy used to calculate α_{shape} for the materials considered were extracted from refs 29−38. As for BeO, GaAs, InAs, and AlN, the γ_l is unknown, we take γ_l equal to 0 J/m^2. As γ_l is always lower than γ_s, taking γ_l as equal to zero in the absence of better information, we get the maximal size effect. Thus, for these materials the α_{shape} obtained represents the upper limit estimation of the size effect.

The lowest value of α_{shape} gives the preferentially adopted shape for isolated nanostructures, considering an isotropic value for the surface tension γ_s. A sphere and a cylinder are the preferentially adopted shapes respectively for nanoparticles and nanowires which is in agreement with the Wulff's construction of nanostructures exhibiting an isotropic surface tension. For other shapes of nanoparticles and nanowires, α_{shape} is always higher than α_{sphere} and $\alpha_{cylinder}$, respectively. Considering the surface tension $\gamma_s(hkl)$ of each crystal face (hkl), the growth rate of the crystal faces, and the influence of the chemical environment on the surface tension of the crystals faces, other shapes may certainly appear experimentally as predicted by the

TABLE 2: Values of the α_{shape} Parameter for Different Shapes of Semiconductors Nanoparticles and Nanowires

			nanoparticle			nanowire ($h = 100$ nm)		
material	atomic no.	$T_{m,\infty}$ (K)	α_{sphere} (nm)	$\alpha_{tetrahedron}$ (nm)	α_{cubic} (nm)	$\alpha_{cylinder}$ (nm)	$\alpha_{parallelepiped}$ (nm)	$\alpha_{hexagonal}$ (nm)
Si	14	1687	1.16	5.69	2.32	0.78	1.56	0.91
Ge	32	1211	1.72	8.45	3.45	1.17	2.32	1.35
BeO		2800	2.04	10.00	4.08	1.38	2.75	1.60
ZnO		2248	3.56	17.43	7.12	2.40	4.79	2.79
CdS		1748	0.38	1.84	0.75	0.25	0.50	0.29
GaAs		1510	1.60	7.85	3.20	1.08	2.16	1.25
InAs		1215	1.71	8.37	3.41	1.15	2.30	1.34
AlN		3273	0.45	2.22	0.91	0.31	0.61	0.35
$TiO_{2\ (rutile)}$		2143	2.58	12.64	5.16	1.74	3.47	2.02

Wulff's construction. Moreover by tuning the chemical environment of the nanostructures, it is possible to favor the growth of one particular shape over another because we can decrease the surface tension relative to the isotropic value γ_s.

Comparing the α_{shape} parameter obtained in this work for materials given in Table 1, with our results previously obtained for supported nanostructures where the melting temperature was calculated, considering the influence of the substrate,[28] we can say that the influence of the silicon substrate is to decrease the value of α_{shape} as noted also by Lee et al. and Kuo et al., respectively.[18,19] Despite the distortion of the sphere shape due to the substrate influence eq 2 can still provide a good estimation for supported spherical nanoparticles with the same α_{shape} parameter calculated from the unsupported case, using L equal to the radius of the effective sphere. The effective sphere is determined from the sphere that has the same curvature as the supported nanoparticle. This has been shown by molecular dynamics simulation performed by Ding et al.[9] However, the influence of the substrate appears especially for non-spherical shapes due to specific terms in eq 2 considering the contact between the surface of the nanostructure with the substrate,[28] which implies that the size effects for isolated free-standing nanostructures are higher than those observed for supported ones.

2.3. Discussion Concerning the Trend between the Bulk Melting Temperature of the Transition Metals and the Size Effect. Considering only transition metals from Table 1, let us plot the bulk melting temperature and the α_{sphere} parameter versus the atomic number (Figure 1a). The materials are organized in three groups, each one corresponding to a specific row in the periodic table of elements. Along each row, the melting temperature increases with the atomic number, then reaching a maximum value and then decreases again due to the filling of orbital "d" in the transition metals before filling of orbital "p" (Hund's rule).[39] Let us explain in more details the melting temperature behavior in terms of orbitals filling. In the fourth row of the periodic table, the transition metals involve the 3d and 4s atomic orbitals. For Sc (Ar)$3d^1 4s^2$, Ti (Ar)$3d^2$-$4s^2$, V (Ar)$3d^3 4s^2$, and Cr (Ar)$3d^5 4s^1$, the 3d atomic orbital is filling and as the 3d orbital is energetically more stable than the 4s orbital for materials with an atomic number higher than 20,[39] the melting temperature increases with the atomic number. Then for Mn (Ar)$3d^5 4s^2$, compared to Cr, the supplementary electron is added in the 4s orbital, that is why the melting temperature of Mn is lower than the melting temperature of Cr. For Fe (Ar)$3d^6 4s^2$, Co (Ar)$3d^7 4s^2$, Ni (Ar)$3d^8 4s^2$, and Cu (Ar)$3d^{10} 4s^1$, the 3d orbital is filling again; but as the number of electrons increases they are more far away from the nucleus than in Sc, Ti, and V and then the melting temperature decreases with the atomic number. For Zn (Ar)$3d^{10} 4s^2$, the same kind of behavior occurs as for Mn; therefore, Zn has a lower melting temperature than Cu. In the fifth row and sixth row of the periodic table, the transition metals involve the 4d−5s and 5d−6s atomic orbitals respectively. The same kind of reasoning can be applied.

Within a row, the α_{sphere} parameter decreases, reaches a minimum value and then increases again. Therefore, α_{sphere} and $T_{m,\infty}$ follow opposite behaviors. In the fourth row, there are three materials which deviates from this trend : Fe, Co and Zn. According to the trend, α_{sphere}(Fe) and α_{sphere}(Co) are expected to be below α_{sphere}(Mn) and α_{sphere}(Ni) due to the higher bulk melting temperature of Fe and Co compared to Mn and Ni. For the same reason, in the case of Zn, α_{sphere}(Zn) is expected to be higher than α_{sphere}(Cu). In the fifth row, there is no deviation from the trend. In the sixth row, W has the higher bulk melting temperature among the transition metals therefore it is expected to have the lowest α_{sphere}. This is not the case, then we suspect some deviations for Re, Os, and Ir. This trend that we have noted for α_{sphere} applies also for the other shapes considered in Table 1.

To show the relation between the material parameters of eq 1 with the atomic number Z, let us plot in Figure 1b, the melting enthalpy, liquid and solid surface tensions versus Z. Within a row, the melting enthalpy, liquid and solid surface tensions, first increases with Z, then reaches a maximum value and finally decreases again. The difference between the liquid surface tension and the solid surface tension follows an opposite behavior, and comparing Figure 1a,b, one can conclude that the highest is the bulk melting temperature the lowest the difference between the liquid surface tension and the solid one. From Figure 1b, we can say that the deviation noted in Figure 1a comes from the behavior of the melting enthalpy of the transition metals with Z. Indeed the deviations in the fourth and sixth rows can be explained by the fact that the maxima of the melting enthalpy and bulk melting temperature are reached at different values of Z. Nevertheless, the deviation of Zn cannot be explained by this way. A possible explanation is to consider the size effect on the melting enthalpy of Zn which will decrease the melting enthalpy[26,27] and will increase the α_{shape}.

Therefore, it is clear from the previous discussion (Figure 1a,b) that for transition metals belonging to the same row in the periodic table, the highest the bulk melting temperature ($T_{m,\infty}$) the smaller the size effect (α_{shape}).

3. Thornton & Hoffman's Criterion at the Nanoscale

As a general case the total residual stress within a material is the sum of two components: intrinsic and thermal. The intrinsic component is due to the growth process itself, whereas the thermal one appears due to the difference between the thermal expansion coefficients between the deposited material and substrate.[40−45] The Thornton & Hoffman's criterion traditionally separates the materials into two categories: the low melting point materials ($T_{substrate}/T_{m,\infty} > 0.25$) and the high

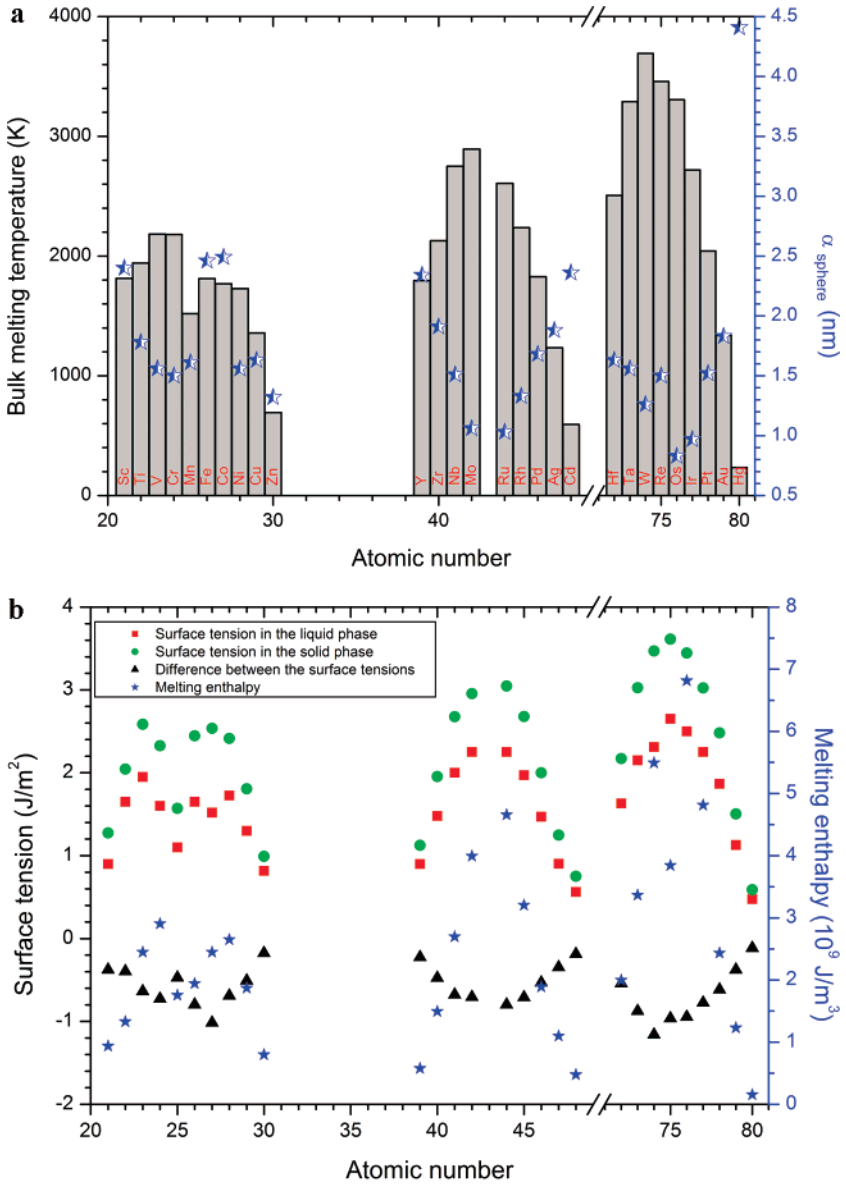

Figure 1. (a) Bulk melting temperature and α_{shape} parameter for a sphere versus the atomic number of materials given in Table 1. The materials are organized in three groups, each one corresponding to a specific row of transition metals in the periodic table. (b) Surface tension and melting enthalpy versus the atomic number of materials given in Table 1. The materials are organized in three groups, each one corresponding to a specific row of transition metals in the periodic table.

melting point materials ($T_{substrate}/T_{m,\infty} < 0.25$).[41] The low/high melting point materials are characterized by a low/high intrinsic residual stress compared to the thermal one. In brief, the separation point at ~0.25 is only valid at the macroscale, since this value is a function of the nanostructures size due to the size effects on the melting temperature. Therefore, the Thornton & Hoffman's criterion can be generalized at the nanoscale according the following equation:

$$T_{substrate}/T_m = 0.28 + 0.31L^{-1} \quad (3)$$

where L is expressed in nanometers.

This relation provides the separation point as a function of the nanostructure size. For details concerning the establishment of this equation the reader is invited to a previous work.[40] Combining eqs 2 and 3, we obtain

$$T_{substrate}/T_{m,\infty} + 0.14\alpha_{shape}L^{-1} + 0.16\alpha_{shape}L^{-2} = 0.28 + 0.31L^{-1} \quad (4)$$

where L is expressed in nanometers. So the term $(0.31 - 0.14\alpha_{shape})L^{-1} - 0.16\alpha_{shape}L^{-2}$, where the size effects are included, allows the Thornton & Hoffman's criterion to be generalized down to the nanoscale. When this term tends to zero (large values of L), we retrieve the Thornton & Hoffman's criterion at the macroscale. Note that the value of the separation point at the macroscale originally proposed (~0.25) is not a strict value; it may vary between 0.2 and 0.3 as discussed by Thompson.[44]

4. Phase Transition Stress Model at the Nanoscale

From the discussion above it becomes clear that the intrinsic residual stress becomes more relevant at the nanoscale due to the shift of the separation point.[40] Therefore, it is important to be able to evaluate this source of stress in nanostructures as nanoparticles, nanowires and thin films.

4.1. Theory. The phase transition stress model treats the intrinsic residual stress as originated from a liquid−solid phase transition. Let us assume that the nanostructure first grows in

TABLE 3: Values of the *k* Parameter for Various Nanostructures Shapes

nature	nanoparticle	nanowire	thin film
nanostructure dimensionality	0D	1D	2D
k	$1/(1-2\nu)$	1	$1/(1-\nu)$

the liquid state. When the nanostructure grows above a critical size, it reaches the solidification temperature. Therefore we propose that the strain generated by this phase transition can be evaluated by considering the thermal shock the nanostructure is subjected. This component is a function of the difference between the melting temperature at the nanoscale, T_m, and the deposition temperature, T_{dep}. In order to give the upper limit of the strain, we consider the highest possible temperature difference, which corresponds to $T_{dep} \approx T_{room}$. Thus, the intrinsic liquid−solid phase transition strain is given as

$$\epsilon = \alpha_f(T_m - T_{room}) \tag{5}$$

where α_f is the thermal expansion coefficient, considered constant with size and temperature [K^{-1}].

The stress corresponding to the intrinsic residual strain evaluated by eq 5 is calculated by eq 6

$$\sigma = kE\epsilon \tag{6}$$

where ϵ is the strain calculated by eq 5, E is the Young's modulus of the material [Pa] (considered constant with size and temperature), and k is an adimensional parameter determining whether we are dealing with uniaxial, biaxial or triaxial stress state (Table 3). A nanowire, a thin film and nanoparticle are examples of uniaxial, biaxial, and triaxial stress states, respectively.

4.2. Discussion Concerning the Inverse Hall-Petch Relation. The basic concept behind this model is that a liquid state is free of stress, and it is when solidification occurs that the intrinsic stress appears due to the change in density between the liquid and the solid state. It explains the intrinsic residual stress during the first steps of solidification due to the appearance of hardness in the material. As reported by other authors, the consequence of this stress at the nanoscale is a reduction of the lattice parameter with size compared to the bulk.[46,47] Generally as the grain size decreases the yield stress and hardness increases, this is known as the Hall-Petch relationship. However there is a deviation from this behavior, known as the inverse Hall-Petch effect, the hardness increases with size at the nanoscale, for sizes below ~15 nm.[48−50] This can be understood by the model proposed in this paper. For sizes below 15 nm, both intrinsic stress and hardness increase with the size before some other process such as voids, microcracks, creep, or other material flaws in general. These later effects are not considered here and therefore our model can only explain the inverse Hall-Petch effect until sizes around ~15 nm and not the Hall-Petch effect for size higher than ~15 nm.

5. Calculation of the Intrinsic Residual Strain in a Hexagonal ZnO Nanowire

Using the model described in the previous section, and using the data summarized in Tables 1−3, one can readily estimate the intrinsic stress component for any nanostructured material and/or shape. In Figure 2, the intrinsic strain map, calculated as a function of the wire dimensions, for a hexagonal ZnO nanowire is shown. The graph only focus on the L and h region below 100 nm where there is a significant size effect. The strain decreases with the height and the length side of the hexagonal nanowire. From Figure 2, we can also see that for the small dimensions of the ZnO nanowire the strain is negative which gives a compressive stress. The transition between compressive to tensile begins for $L \approx 2$ nm and $h \approx 7$ nm, in agreement with the range given in.[51,52] This transition can be tuned with the deposition temperature T_{dep}, as evidenced by eqs 7a, 7b, and 8, if instead of $T_{dep} \approx T_{room}$ (which provides the upper limit for the intrinsic strain) one consider the actual deposition temperature. The equations of the contours in Figure 2 are given by

$$\epsilon(L,\alpha_{shape}) = \alpha_f\left\{T_{m,\infty}\left(1 - \frac{\alpha_{shape}}{2L}\right) - T_{room}\right\} \tag{7a}$$

Then eq 7a can be written as function of the hexagonal wire dimensions and basic material parameters

$$\epsilon(L,h) = \alpha_f\left\{T_{m,\infty}\left[1 + \frac{(\gamma_l - \gamma_s)}{\Delta H_{m,\infty}}\left(\frac{4}{L\sqrt{3}} + \frac{2}{h}\right)\right] - T_{room}\right\} \tag{7b}$$

The relation between L and h, for an hexagonal nanowire which determines the border between compressive and tensile stress, i.e., $\epsilon(L,h) = 0$, shown as a dashed red contour in Figure 2 is given by

$$h = 2\left[\left(\frac{T_{room}}{T_{m,\infty}} - 1\right)\frac{\Delta H_{m,\infty}}{(\gamma_l - \gamma_s)} - \frac{4}{L\sqrt{3}}\right]^{-1} \tag{8}$$

Experimental data concerning intrinsic strain evaluation of free-standing nanostructures is scarce making difficult a direct comparison with experiments. Nevertheless, we can compare our results with the fracture strain of hexagonal ZnO nanowires, grown on a silicon substrate, measured by Chen and Zhu.[53] Our calculation gives a lower value of the intrinsic strain (0.005) than the fracture strain (~0.05) which is what is expected since the intrinsic strain should be lower than the fracture strain. Another recent work[54] reports strain in "free-standing" parallelepiped Ge nanowires ($L \sim 30$ nm and $h \sim 100$ nm) and the authors have observed a strain value around 0.002, which is within the same order of magnitude as obtained from our calculations. Thus, so far one can only argue that our results are in good qualitative agreement with the available experimental results recently reported. It will be rather interesting to compare with experimental data in the region where size effects become stronger, i.e., for nanowires with smaller radius.

One should keep in mind that other origins of intrinsic residual stress, exist such as oxidation and impurity incorporation in "real" nanostructures, but all these effects give a compressive stress component to the intrinsic part. Furthermore, there are several relaxation processes such as voids, microcracks, creep or other material flaws in general, which are not considered here. Therefore the phase transition stress model here presented provides an estimation of the upper limit of the intrinsic stress component.

Relatively to the intrinsically preferentially shape adopted by the nanostructures, we also expect deviations. There are three main reasons for this: (1) the chemically active environment during growth, which may change dramatically the surface tension; (2) the anisotropy of the surface tension along different crystallographic planes (Wulff's construction); (3) the different growth rates of the crystal faces.

This deviation occurs, for instance, for ZnO where the most common shape observed experimentally for the NW is the hexagonal (linked to the hexagonal wurtzite type crystal structure), rather than the cylindrical one.[55] Unfortunately, so

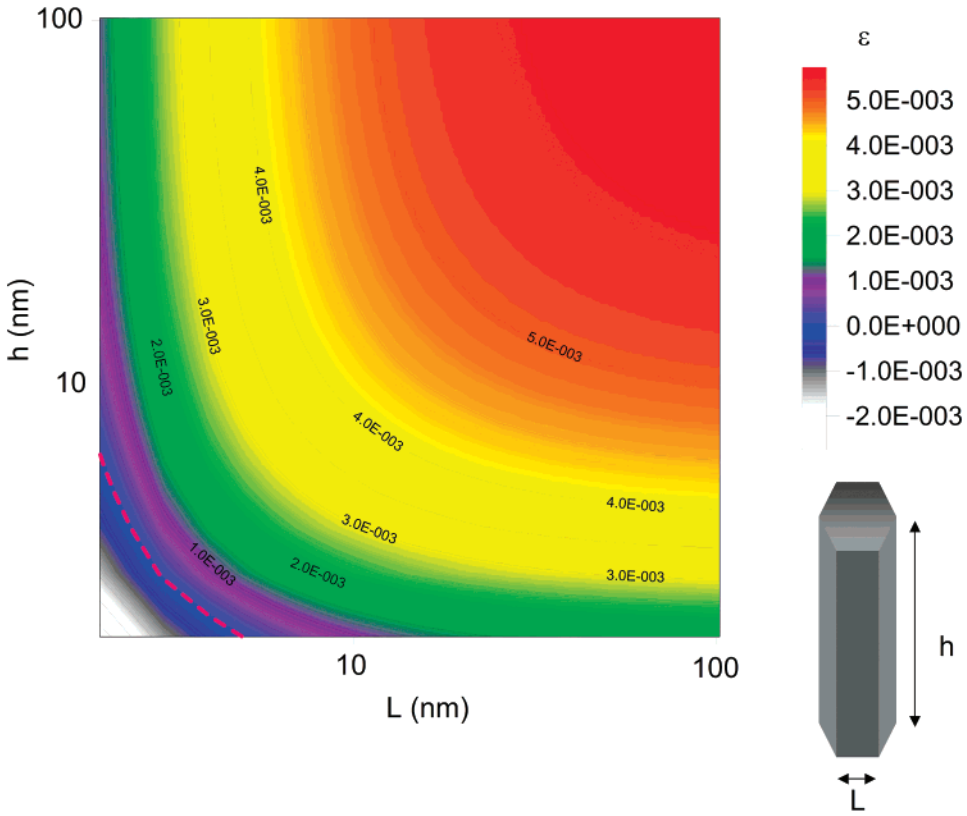

Figure 2. Residual strain of a hexagonal ZnO nanowire versus its dimensions (length h and length side L). The dashed line separates the compressive and the tensile domains. For the calculations we have used the following parameters : $\gamma_s = 3.16$ J/m^2, $\gamma_l = 0.30$ J/m^2, $T_{m,\infty} = 2248$ K, $\alpha_f = 3.02 \times 10^{-6}$ K^{-1}, and $\Delta H_{m,\infty} = 4.82 \times 10^9$ J/m^3.[35,56] T_{room} is taken equal to 293 K.

far, the values of surface tension for the various growth planes are unknown for most nanomaterials.

The simple thermodynamic model here proposed describes the general trends at the nanoscale for a wide range of materials in terms of melting temperature and intrinsic strain. Using the data from Tables 1 and 2, and eqs 2 and 7a, one can easily obtain an estimate of T_m and ϵ, as a function of size and shape. We note that these size and shape effects are only relevant for structures with size below 100 nm, i.e., for nanomaterials.

A more refined formalism including the effects of chemical environment, faces growth rates and the surface tension anisotropy can be developed once the relevant physical parameters are well-known. Before considering relaxation processes at the nanoscale, which will be the scope of another work, this contribution intends to provide an early insight to model intrinsic residual strain at the nanoscale during the first growth steps of nanostructures.

6. Conclusions

At the nanoscale size and shape, effects are relevant parameters that influence basic material properties. Here we have quantitatively estimated these effects on the melting temperature for a large number of nanomaterials. To evaluate these effects, we have defined the α_{shape} parameter which allows the size effect on the melting temperature to be determined conveniently. We have also analyzed the behavior of the α_{shape} parameter with the atomic number and explained why the highest is the bulk melting temperature, the lower the size effect. This trend arises from the surface tension and the bulk melting enthalpy of the transition metals.

Considering the size effect on the Thornton & Hoffman's criterion at the nanoscale we have highlighted the importance of considering intrinsic residual stress for sizes lower than 100 nm. Hence, using the α_{shape} parameter we have proposed a simple phase transition stress model that explains the origin of the intrinsic stress as follows: a liquid state is free of stress and the stress appears during solidification due to the change in density between the liquid and the solid phases. During the first steps of solidification, the intrinsic stress corresponds to the hardness appearance in the material. The model provides an upper limit of intrinsic residual stress for any given nanomaterial and allows the inverse Hall-Petch relation for size below 15 nm to be explained. Nevertheless, it can be refined in order to consider the surface tension anisotropy in nanocrystals, faces growth rates, chemical environment, relaxation processes such as microcracks, voids, creep, or other material flaws, and in order to account for the effects of impurities and oxidation.

This theoretical work is obviously a first approach. The work presented here can be improved considering the size and temperature dependencies of the surface tensions, melting enthalpy, thermal expansion coefficient and Young's modulus. Furthermore, it can be extended to take into account the chemical environment and the anisotropy of the surface tensions. Experimental work to determine the surface tension of the different crystals faces of semiconductors will be highly desirable. At the present stage this factor limits the use of eqs 1−8, and therefore it is difficult to gain a more precise insight regarding the nanoscale behavior of several materials with scientific and technological interest. Work is in progress to consider the size and temperature dependencies of the mentioned properties and to calculate the α_{shape} parameter for other semiconductors and ceramics.

Acknowledgment. The authors would like to acknowledge financial support from Fundação para a Ciência e Tecnologia

(FCT) through the Project PTDC/FIS/65233/2006. G.G. is being funded by an FCT postdoctoral Grant SFRH/BPD/34727/2007.

References and Notes

(1) Timp, G. *Nanotechnology*; AIP Press: New York, 1999.
(2) Yacaman, M. J.; Ascencio, J. A.; Liu, H. B.; et al. *J. Vacuum Sci. Technol. B* **2001**, *19*, 1091.
(3) Wang, Z. L.; Petroski, J. M.; Green, T. C.; et al. *J. Phys. Chem. B* **1998**, *102*, 6145.
(4) Bachels, T.; Guntherodt, H. J.; Schafer, R. *Phys. Rev. Lett.* **2000**, *85*, 1250.
(5) Liu, X.; Yang, P.; Jiang, Q. *Mater. Chem. Phys.* **2007**, *103*, 1.
(6) Takagi, M. J. *Phys. Soc. Jpn.* **1954**, *9*, 359.
(7) Su, X.; Zhang, Z. J.; Zhu, M. M. *Appl. Phys. Lett.* **2006**, *88*, 061913.
(8) Delogu, F. *Nanotechnology* **2007**, *18*, 325706.
(9) Ding, F.; Rosen, A.; Curtarolo, S.; et al. *Appl. Phys. Lett.* **2006**, *88*, 133110.
(10) Pawlow, P. *Z. Phys. Chem.* **1909**, *65*, 1.
(11) Borel, J. P. *Surf. Sci.* **1981**, *106*, 1.
(12) Takagi, M. J. *Phys. Soc. Jpn.* **1986**, *55*, 3484.
(13) Zhao, M.; Zhou, X. H.; Jiang, Q. *J. Mater. Res.* **2001**, *16*, 3304.
(14) Sun, C. Q.; Tay, B. K.; Zeng, X. T.; et al. *J. Phys.-Condensed Matter* **2002**, *14*, 7781.
(15) Nanda, K. K.; Sahu, S. N.; Behera, S. N. *Phys. Rev. A* **2002**, *66*, 013208.
(16) Goldstein, A. N.; Echer, C. M.; Alivisatos, A. P. *Science* **1992**, *256*, 1425.
(17) Yang, C. C.; Li, S. *Phys. Rev. B* **2007**, *75*, 165413.
(18) Lee, J.; Tanaka, T.; Lee, J.; et al. *CALPHAD* **2007**, *31*, 105.
(19) Kuo, C. L.; Clancy, P. *J. Phys. Chem. B* **2005**, *109*, 13743.
(20) Guisbiers, G.; Abudukelimu, G.; Clements, F.; et al. *J. Comput. Theor. Nanosci.* **2007**, *4*, 309.
(21) Abudukelimu, G.; Guisbiers, G.; Wautelet, M. *J. Mater. Res.* **2006**, *21*, 2829.
(22) Wautelet, M. *J. Phys. D* **1991**, *24*, 343.
(23) Wautelet, M. *Eur. Phys. J.* **2005**, *29*, 51.
(24) Wautelet, M. *Phys. Lett. A* **1998**, *246*, 341.
(25) Tolman, R. C. *J. Chem. Phys.* **1949**, *17*, 333.
(26) Liang, L. H.; Zhao, M.; Jiang, Q. *J. Mater. Sci. Lett.* **2002**, *21*, 1843.
(27) Zhang, Z.; Lu, X. X.; Jiang, Q. *Physica B* **1999**, *270*, 249.
(28) Guisbiers, G.; Wautelet, M. *Nanotechnology* **2006**, *17*, 2008.
(29) Kittel, C. *Introduction to solid state physics*; Wiley: New York, 1995.
(30) Trimble, V. *CRC Handbook of Chemistry and Physics*; CRC Press: Boca Raton, FL, 1987.
(31) Vitos, L.; Ruban, A. V.; Skriver, H. L.; et al. *Surf. Sci.* **1998**, *411*, 186.
(32) Keck, P. H.; Vanhorn, W. *Phys. Rev.* **1953**, *91*, 512.
(33) Messmer, C.; Bilello, J. C. *J. Appl. Phys.* **1981**, *52*, 4623.
(34) Gomez, M. A.; Pratt, L. R.; Kress, J. D.; et al. *Surf. Sci.* **2007**, *601*, 1608.
(35) Martienssen, W.; Warlimont, H. *Springer Handbook of Condensed Matter and Materials Data*; Springer: Berlin, 2005.
(36) Li, Y. L.; Ishigaki, T. *J. Cryst. Growth* **2002**, *242*, 511.
(37) Zhang, H. Z.; Banfield, J. F. *J. Mater. Chem.* **1998**, *8*, 2073.
(38) Zhang, H. Z.; Banfield, J. F. *J. Phys. Chem. B* **2000**, *104*, 3481.
(39) Atkins, P. W. *Chimie générale*; Intereditions, Paris, 1992.
(40) Guisbiers, G.; Van Overschelde, O.; Wautelet, M. *Acta Mater.* **2007**, *55*, 3541.
(41) Thornton, J. A.; Hoffman, D. W. *Thin Solid Films* **1989**, *171*, 5.
(42) Koch, R. *J. Phys.-Condensed Matter* **1994**, *6*, 9519.
(43) Doerner, M. F.; Nix, W. D. *CRC Crit. Rev. Solid State Mater. Sci.* **1998**, *14*, 225.
(44) Thompson, C. V.; Carel, R. *J. Mech. Phys. Solids* **1996**, *44*, 657.
(45) Windischmann, H. *Crit. Rev. Solid State Mater. Sci.* **1992**, *17*, 547.
(46) Lamber, R.; Wetjen, S.; Jaeger, N. I. *Phys. Rev. B* **1995**, *51*, 10968.
(47) Qi, W. H.; Wang, M. P. *J. Nanopart. Res.* **2005**, *7*, 51.
(48) Pande, C. S.; Masumura, R. A. *Mater. Sci. Eng. A* **2005**, *409*, 125.
(49) Zhao, M.; Li, J. C.; Jiang, Q. *J. Alloys Compd.* **2003**, *361*, 160.
(50) Sanders, P. G.; Eastman, J. A.; Weertman, J. R. *Acta Mater.* **1997**, *45*, 4019.
(51) Cammarata, R. C.; Trimble, T. M.; Srolovitz, D. J. *J. Mater. Res.* **2000**, *15*, 2468.
(52) Floro, J. A.; Chason, E.; Cammarata, R. C.; et al. *MRS Bull.* **2002**, *27*, 19.
(53) Chen, C. Q.; Zhu, J. *Appl. Phys. Lett.* **2007**, *90*.
(54) Taraci, J. L.; Hytch, M. J.; Clement, T.; et al. *Nanotechnology* **2005**, *16*, 2365.
(55) Wang, Z. L. *J. Phys.-Condensed Matter* **2004**, *16*, R829.
(56) Jiang, J. Z.; Olsen, J. S.; Gerward, L.; et al. *Europhys. Lett.* **2000**, *50*, 48.